

Tackiness and cohesive failure of granular pastes: Mechanistic aspects

Y.O. Mohamed Abdelhaye^{1,a}, M. Chaouche², J. Chapuis³, E. Charlaix⁴, J. Hinch⁵, S. Roux², and H. Van Damme^{6,7,b}

¹ College of Sciences and Arts, Al Jouf University, P.O. Box 756, Al-Qurayat, Saudi Arabia

² Laboratoire de Mécanique et Technologie, Ecole Normale Supérieure de Cachan/CNRS-UMR 8535, 61 Avenue du Président Wilson, F-94235 Cachan Cedex, France

³ Lafarge Centre de Recherche, rue du Montmurier, 38291 Saint Quentin Fallavier, France

⁴ LPMCN, UMR 5586, Université Claude Bernard, Lyon I, 43 Boulevard du 11 novembre 1918, 69622 Villeurbanne Cedex, France

⁵ DAMTP, University of Cambridge, Wilberforce Road, Cambridge CB3 0WA, UK

⁶ ESPCI-ParisTech, 10 rue Vauquelin, 75231 Paris cedex 05, France

⁷ Université Paris Est, IFSTTAR, 58 boulevard Lefebvre, 75732 Paris Cedex 15, France

Received 3 October 2011 and Received in final form 21 April 2012

Published online: 14 June 2012 – © EDP Sciences / Società Italiana di Fisica / Springer-Verlag 2012

Abstract. Granular pastes are dense dispersions of non-colloidal grains in a simple or a complex fluid. Typical examples are the coating, gluing or sealing mortars used in building applications. We study the rupture of a thick layer of mortar paste in a simple pulling test where the paste is confined between two flat surfaces. It is shown that, depending on the rheological properties of the paste and the plate separation velocity, two main failure modes are obtained. The first mode is the inwards shear flow of the paste with viscous fingering instabilities, similarly to what has been observed with Newtonian fluids and with non-Newtonian colloidal suspensions or polymer solutions. The second failure mode is stemming from the expansion of bubbles, similarly to what has been observed in soft adhesive polymer layers and, more recently, in highly viscous fluids. It is shown that the crossover between the two failure modes is determined by the conditions required to generate a pressure drop able to trigger the growth of pre-existing micro-bubbles smaller than the inter-granular distance.

1 Introduction

The extensional deformation of a thin layer of a pasty complex fluid (polymer melt, polymer solution, colloidal suspension, granular paste) confined between two surfaces is a type of flow encountered in numerous situations. A familiar case is the separation of two surfaces bonded by a layer of fresh glue or of soft adhesive (tape, labels, Post-It note[®]), or the withdrawal of the tool (brush, trowel, knife) used to spread paint or mortar on a wall, or even more simply, marmalade or butter on bread. The questions raised by this type of flow have led to two types of model studies. On one hand, a number of studies with Newtonian or non-Newtonian liquids focused on the instabilities which are developing as the plates confining the fluid are separated at constant velocity [1–8]. Indeed, since air is entering the gap between the plates as the more viscous fluid recedes towards the center, the Saffman-Taylor instability is unavoidably occurring [9]. The analytical approach to

this instability is made extremely complex by the time-dependent plate separation, but the assumption is usually made that the Darcy approximation is still valid. Even with this assumption, the problem is significantly different from the classical Saffman-Taylor problem at constant plate separation [8]. Using yield-stress fluids makes it even more different by introducing a strong pinning effect of the interface [10].

On the other hand, a large number of studies have been devoted to the separation of two surfaces bonded by a layer of soft or “pressure-sensitive” adhesive [11,12]. Pressure sensitive adhesives (PSAs) are polymers designed to stick on almost any surface by simple contact under light pressure. Most of them are formulated (co)polymer blends with a glass transition temperature well below their usage temperature [11]. Their very sticky character, or “tackiness”, is due to the combination of a large maximum force required to separate the surfaces and to a large energy dissipated during this process. Debonding arises through a complex mechanism involving heterogeneous cavitation, in parallel to possible (and limited) viscous fingering start-

^a e-mail: my.abdelhaye@ju.edu.sa

^b e-mail: henri.van-damme@ifsttar.fr



Fig. 1. One of the two failure surfaces obtained by separating two 30 cm \times 30 cm glass plates between which a 2 cm thick granular adhesive paste was confined (paste P_β , sect. 2.1) (from [19], with permission).

ing from the boundaries [11, 13–16]. As the bubbles grow, the walls between them become thinner and finally turn into fibrils which elongate until fracture. Thus, whereas the case of Newtonian or non-Newtonian fluids is usually treated as a pseudo-2D Saffman-Taylor problem, the case of soft adhesives is treated as a fully 3D problem [17].

Recently though, experiments were conducted with highly confined Newtonian liquids (silicone oils) at large plate separation rate [18, 19]. In that case, a transition from Poiseuille flow —eventually altered by fingering instabilities— to heterogeneous cavitation was also observed. This shows that, in a parameter space which remains to be defined, a common framework for the debonding mechanisms in simple and complex fluids may be looked for.

In this paper, we focus on the case of pastes. Colloidal and granular pastes may be defined as very dense dispersions of colloidal or non-colloidal particles, respectively. The dispersion medium may be a simple liquid or a complex fluid itself (a polymer solution for instance) [20]. The packing density is approaching the jamming situation. With respect to other complex fluids or soft solids, pastes are often characterized by a marked plastic character, *i.e.* by their ability to withstand large strains at constant stress (think of clay putty or wet sand for instance). The strain dependence of the pulling force in plane-plane debonding experiments has recently been studied, using cement-based mortar pastes [21, 22].

In a preliminary work [23, 24] we explored some morphological aspects of the fracture profiles obtained in plane-plane debonding experiments performed with granular adhesives (crushed sand in an acrylic resin), at fixed particle concentration. Fracture was shown to be cohesive (*i.e.* occurring within the paste layer) and highly ductile, after a plastic deformation large with respect to the initial layer thickness but still small compared to the plate size. Though not really similar to that of PSAs, the morphology of the failure surfaces was suggesting a failure mechanism combining moderate inwards flow and a more extensive internal growth of voids (fig. 1).

In the present work, we report additional experiments performed with granular pastes at variable grain concentration and rheological properties, focusing on the failure mode. Changing these variables, we were able to go deeper into the failure mechanism and to explore failure modes going from the inwards flow-controlled mode to the de-

fect or void-controlled mode. Due to the almost randomly close-packed density of grains in the medium, flow of the dispersion fluid in granular pastes has an intrinsic length scale which is the average size of the void space between grains. We show semi-quantitatively that the onset of the void-controlled fracture mode corresponds to the conditions for capillary invasion in this void space.

2 Experimental

2.1 Materials

The main set of experiments was performed using ten different paste batches prepared in Lafarge Central Laboratory (Lafarge LCR) by mixing crushed quartz sand (average particle diameter around 30 μm), water and cellulose derivatives. These pastes, which will be referred to as the P_α paste samples in the following, were not hardening (as they would, if quartz were replaced by cement, like in ordinary mortars). By changing slightly the composition, pastes with different rheological behaviors could be prepared. The set P_α was used to explore the transition between the different failure modes. The detailed chemical composition of the pastes is of little importance since the correlation we are seeking for is between the paste rheological properties, the conditions of the debonding experiment and the failure mode. The rheological behavior of each paste was characterized in simple shear flow using a stress-controlled instrument equipped with a so-called Vane tool (a six-bladed tool rotating concentrically with a fixed cylinder). A noticeable feature observed for all samples is the absence of yield stress. All pastes were shear-thinning and for seven pastes out of the ten, the shear stress *vs.* shear rate curves could be reasonably well fitted with a simple power law up to shear rates approaching 5 s^{-1} :

$$\tau = K\dot{\gamma}^\alpha. \quad (1)$$

In this equation τ is the shear stress, $\dot{\gamma}$ is the shear rate, and K and α are adjustable parameters. The values of K and α for these seven pastes are summarized in table 1. The exponent α is close to 0.3 for all samples.

In addition to the lab-prepared pastes just described, a commercial granular adhesive was also used, as received in closed pots from Produits chimiques du Nord (technical notice 13/91.536 from the CSTB, the French Scientific

Table 1. Rheological parameters (“ α ” and “ K ” columns) and summary experimental results (all other columns) characterizing the paste samples (from $P_{\alpha 1}$ to $P_{\alpha 10}$) and the small-scale debonding experiments. α and K are the shear-thinning exponent and consistency parameter, respectively, obtained by fitting the flow curves of the seven P_{α} paste batches with a power law shear stress *vs.* shear rate relationship (eq. (1)). D is the plate diameter and h is the initial gap between plates in the debonding experiments. The results are summarized as “ XX (Y) ZZ ” sets. XX is the peak pulling force values [N]; (Y) is the failure modes (A , B or C); ZZ is the ratio between the calculated and the observed peak pulling force ($F_{\max\text{-cal}}/F_{\max\text{-obs}}$).

	α	K	$D = 32$ mm			$D = 75.5$ mm		
			$h = 0.5$ mm	$h = 1.0$ mm	$h = 1.5$ mm	$h = 0.5$ mm	$h = 1.0$ mm	$h = 1.5$ mm
$P_{\alpha 1}$	4.0 (A) ...	1.9 (A) ...	1 (A) ...	56.6 (B) ...	28.5 (g) ...	16.7 (g) ...
$P_{\alpha 2}$	7.4 (C) ...	4.0 (C) ...	2.4 (C) ...	85.1 (C) ...	45.7 (C) ...	31.4 (C) ...
$P_{\alpha 3}$	0.30	101	1.3 (A) 3.49	0.8 (A) 1.87	0.5 (A) 1.56	21.4 (B) 3.68	10.4 (B) 2.50	6.5 (B) 2.09
$P_{\alpha 4}$	0.1 (A) ...	0.1 (A) ...	0.2 (A) ...	3.1 (A) ...	1.6 (A) ...	2.0 (A) ...
$P_{\alpha 5}$	0.26	460	11.8 (C) 1.57	4.4 (C) 1.47	2.6 (C) 1.35	107.2 (B) 2.91	52.4 (B) 2.07	36.2 (A) 1.62
$P_{\alpha 6}$	0.27	351	6.6 (B) 2.21	2.6 (A) 1.93	1.3 (A) 2.06	96.6 (B) 2.55	50.2 (B) 1.69	25.4 (A) 1.79
$P_{\alpha 7}$	0.30	165	3.4 (B) 2.18	1.4 (A) 1.75	0.7 (A) 1.83	55.1 (B) 2.33	22.9 (B) 1.85	13.7 (A) 1.62
$P_{\alpha 8}$	0.44	76	2.0 (A) 2.44	0.8 (A) 1.66	0.4 (A) 1.54	32.1 (B) 2.98	14.9 (A) 1.74	8.4 (A) 1.44
$P_{\alpha 9}$	0.33	131	3.3 (B) 1.93	1.6 (B) 1.26	0.8 (B) 1.28	55.7 (B) 2.04	21.9 (B) 1.64	13.5 (A) 1.36
$P_{\alpha 10}$	0.32	187	6.7 (C) 1.32	3.4 (C) 0.84	2.3 (C) 0.63	71.6 (C) 2.18	46.1 (C) 1.09	29.5 (C) 0.87

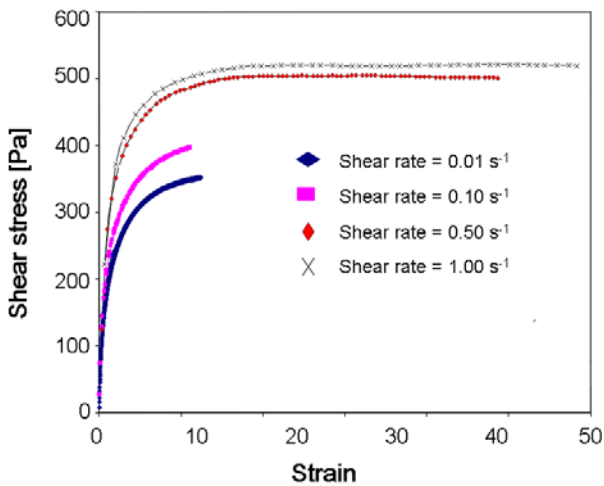


Fig. 2. Shear stress *vs.* shear strain curves at different strain rates, obtained with the granular adhesive paste used in fig. 1 (sample P_{β}).

and Technical Center for Buildings). This pasty granular adhesive, which will be referred to as the P_{β} sample in the following, is the same as that used in our preliminary study of failure surface morphology [23]. It is made of crushed calcareous sand saturated with a water-based acrylic polymer resin which is hardening when contacted with air. The hardening time was of the order of several hours, which is giving ample time to perform debonding experiments without significant evolution of the rheological behavior. The main rheological feature of this paste is its good stability (no solid-liquid segregation, even under pressure) and visco-plasticity. This visco-plastic character is easily evidenced by measuring the stress-strain relationship in imposed shear rate conditions, using a Vane tool in order to avoid any slippage. Indeed, as illustrated in

fig. 2, the stress-strain curves for this paste are characterized by 1) a very limited (in terms of strain) close-to-linear rise of the stress at small strain, and 2) a stress plateau at large strain. It is tempting to associate these two responses with an elastic response and a plastic response, respectively, but their strain rate dependence shows that it is not that simple. Both features exhibit a strain rate dependence, as illustrated in fig. 2. This shows that the initial regime can in no way be considered as a purely elastic response. It also shows that the stress at large strain, in the pseudo-plastic regime, has a significant viscous component. However, the very weak dependence of the stress on the strain rate (stress plateau \sim strain rate^{0.3}) suggests that the plastic contribution is the major one. Due to this behavior and to its characteristic failure surface morphology which exhibits a mixture of highly deformed and much less deformed regions, paste P_{β} was used to explore the PSA-like cohesive failure mechanism.

2.2 Methods

Debonding experiments (or “probe tack tests” in PSA terminology) were performed as follows, using either 1) a home-made hydraulic setup or 2) a general purpose traction-compression INSTRON test machine, or 3) a stress-controlled shear rheometer with normal force measurement capacity (AR2000 from TA Instruments). With the P_{α} samples, stainless steel circular plates ($D = 32$ or $D = 75$ mm) were used with the test machine. With the granular adhesive (P_{β} sample), two circular and transparent PMMA (Plexiglas) plates of diameter $D = 90$ mm were used with the home-made setup. Two stainless steel plates ($D = 40$ mm) were used with the rheometer and two other stainless steel plates ($D = 80$ mm) with the general purpose test machine. In either case, a given amount

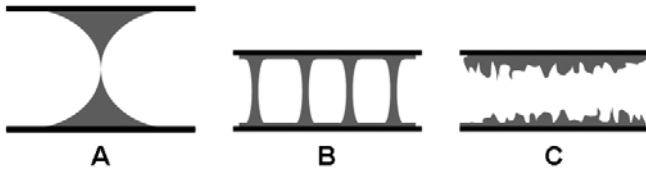


Fig. 3. Cartoon illustrating schematically the three different failure modes which were observed with the P_α paste samples.

of paste was placed on the lower plate. The upper plate was then pressed on the paste until a given gap h was reached ($h = 0.5, 1.0$ or 1.5 mm for the P_α samples and $1 \leq h \leq 10$ mm for the P_β sample). The excess paste on the boundary was then removed and the upper plate was lifted at a constant velocity $\dot{h} = dh/dt$. We used $\dot{h} = 6 \times 10^{-4} \text{ m s}^{-1}$ with the P_α samples in the test machine; $1.5 \times 10^{-5} \leq \dot{h} \leq 2.5 \times 10^{-4} \text{ m s}^{-1}$ with the granular adhesive P_β in the home-made setup, $1.5 \times 10^{-3} \leq \dot{h} \leq 8 \times 10^{-3} \text{ m s}^{-1}$ with P_β in the test machine, and $1.0 \times 10^{-5} \leq \dot{h} \leq 6 \times 10^{-4} \text{ m s}^{-1}$ with P_β in the rheometer. The whole force *vs.* displacement curve was recorded with the P_β sample whereas only the maximum force was recorded with the P_α samples.

The debonding mode was qualitatively determined by observing the profile of the paste layer and the paste surface after debonding. Three different debonding modes could be identified in the experiments performed with the P_α samples, the appearance frequency of which will be reported in sect. 3. In mode *A*, the paste was flowing towards the center of the plates and the pattern just before debonding is a central and narrowing paste column. In mode *B*, several narrow columns are formed, much like with very soft PSAs, and a thin layer of paste is remaining on (almost) the total plate surfaces. Finally, in mode *C*, a thin and homogeneous but very rough and prickly layer of paste remains on each plate. Modes *B* and mode *C* are clearly akin to each other. Those three modes are sketched in fig. 3.

In summary, each debonding experiment is characterized by a set of four control parameters: the type of paste, P_α or P_β ; the plate diameter, D ; the gap, h , and the separation velocity, $\dot{h} = dh/dt$. The result is characterized by the failure mode, M , and the maximum force needed for debonding (or the whole force *vs.* displacement curve for the P_β samples). Thus, with the P_α samples, a total of $10(P_\alpha) \times 2(D) \times 3(h) \times 1(\dot{h}) = 60$ experiments were performed. With the P_β sample, fourteen experiments were performed with the home-made setup and fourteen others with the test machine, differing by the initial thickness h_0 of the layer and the separation velocity \dot{h} , and seven experiments were performed with the rheometer, differing only by the separation velocity.

3 Results and discussion

Whatever the type of paste and the type of debonding experiment, failure was always found to be cohesive, that

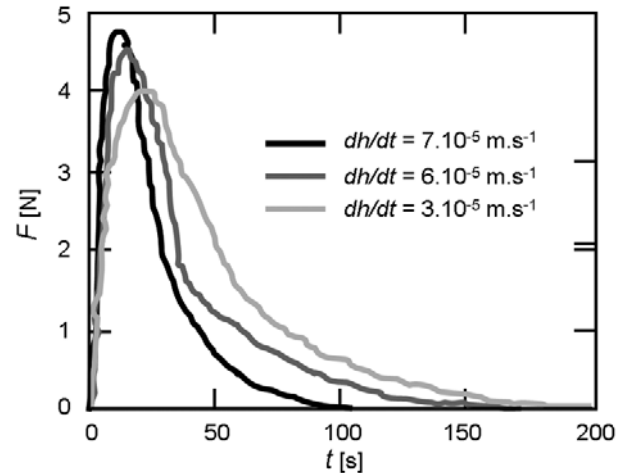


Fig. 4. Examples of pulling force *vs.* time (linearly related to displacement) curves obtained with the granular adhesive paste (sample β) at three different separation velocities. Notice the weak velocity dependence of the maximum pulling force.

is, occurring within the layer of paste. The typical shape of the force curves (P_β samples set) was qualitatively the same as previously reported for debonding experiments performed with simple or complex fluids [18, 19, 21, 22, 25]. The force first increases as the fluid layer and experimental setup are put in tension. It passes through a maximum, F_{\max} , and then decreases as inward flow or/and rupture starts (fig. 4). It should be noted that, as pointed out in [19] and in [26], the occurrence of a maximum is, generally speaking, the signature of the machine compliance. With an infinitely rigid machine, the force would start at a finite value and always decrease as the plate separation increases, as we shall see. In pasty fluids like ours, which are very difficult to prepare without entrapping some air, the fluid compressibility is an additional factor to take into account. Just like the machine compliance, it leads to a “softer” mechanical response of the system.

We will start by analyzing the results obtained with the P_α samples in terms of failure mode and go deeper into the PSA-like mode with the P_β sample thereafter.

3.1 From Poiseuille flow to heterogeneous cavitation

Table 1 summarizes the maximum pulling force values, F_{\max} , and failure modes obtained with the P_α paste set. All three types of failure modes have been observed. Small maximum force values tend to be associated with the debonding mode *A*, similar to what is observed with simple liquids (inwards flow towards the center, possibly with fingers [8]). Large values tend to be associated with failure modes *B* and *C*, akin to what is observed with soft adhesives (fibrillation [11]). However, the correlation is not as straightforward as that, as may be noticed by carefully scrutinizing table 1. Hence, a criterion better than F_{\max} has to be looked for.

With soft adhesives, the initial step leading to fibrillation was first believed to be cavitation at the adhesive-

plate interface, triggered by the microscopic plate roughness [11, 15]. Later, it was shown that cavitation was more probably triggered by air bubbles initially trapped into the bulk of the adhesive layer during the deposition process, while surface roughness was triggering interfacial cracks rather than bulk cavitation [27].

In the present case of granular pastes, if bubbles grow and lead to failure, they are in the bulk of the paste layer. Otherwise, clean (*i.e.* paste-free) spots would have been observed on the plates. The parameters controlling the growth of bubbles are the Laplace pressure in the bubbles on the one hand, and the viscous flow-induced pressure drop (“suction”) in the paste, $|p_{\min} - p_{\text{atm}}|$, on the other hand. In order to calculate the flow-induced pressure drop, a constitutive law for the rheological behavior of the paste is needed, in conjunction with a flow model. This is possible for the seven pastes which follow eq. (1) in shear flow.

Using a lubrication-type approach, Meeten [28] has shown that the pulling force, F , is related to the rheological parameters of the paste, K and α , to the plate radius $R = D/2$ and to the plate separation rate \dot{h} by

$$F = 2\pi K \frac{(2 + 1/\alpha)^\alpha \dot{h}^\alpha R^{3+\alpha}}{(3 + \alpha) h^{1+2\alpha}}, \quad (2)$$

$F = F_{\max}$ when $h = h_0$, the minimum plate separation at the start of the debonding experiment. Knowing F_{\max} , the maximum pressure drop in the paste layer follows:

$$\Delta p_{\max} = |p_{\min} - p_{\text{atm}}| = \frac{(3 + \alpha) F_{\max}}{(1 + \alpha) \pi R^2}. \quad (3)$$

The use of lubrication theory in shear flow is *a priori* a questionable assumption. Indeed, the flow of a fluid between two plates moved away from each other differs from a simple shear. Depending on the boundary conditions, either a lubricational or an elongational regime can be obtained. When the layer is thin compared to the plate radius (highly confined conditions), the first regime should be obtained while if the layer is thick or with perfect slip on the walls the second regime should be obtained. No evidence for wall slip was observed in our experiments and, at least in failure mode *B* or *C*, the onset of failure was always occurring at a plate separation small compared to the plate radius. We may therefore consider that, whilst some regions of the paste may experience extensional deformation, most of the flow is occurring in a lubrication regime. This is a significant difference with respect to PSA adhesives, which are extensively elongated in fibrils before failure.

As shown in table 1 and fig. 5, with $\dot{h} = 6.10^{-4} \text{ m s}^{-1}$, the agreement between the calculated and the measured values of F_{\max} ($F_{\max,\text{calc}}$ and $F_{\max,\text{obs}}$, respectively) is reasonably good. Therefore, a first conclusion in agreement with other studies on colloidal or granular pastes [10, 18, 19, 21, 22, 25], is that the viscous force —*i.e.* the force required to force the viscous flow of the paste— is the major contribution to the pulling effort. Considering the very weak dependence of F_{\max} on the separation

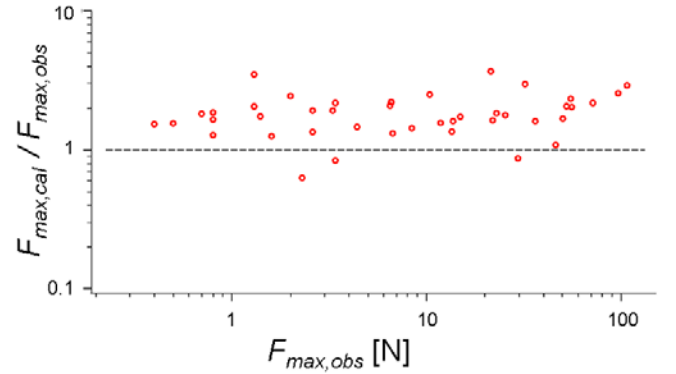


Fig. 5. Comparison between the calculated and measured maximum pulling force in the experiments performed with pastes P_α .

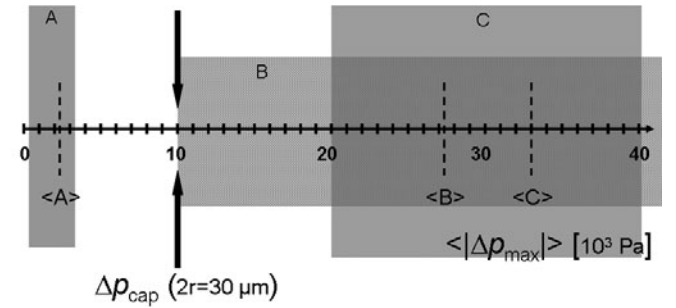


Fig. 6. Schematic summary, along the horizontal axis, of the distribution of maximum depression values during the debonding experiments. Each grey rectangle includes all the values calculated from the maximum pulling forces for a given failure mode (the vertical direction has no physical significance and has been introduced for the sake of clarity). The vertical dashed lines indicate the average depression for each mode. The facing black arrows indicate the Laplace (or capillary) pressure at the onset of mode *B*.

rate \dot{h} ($F_{\max} \propto \dot{h}^\alpha$, with $\alpha \cong 0.3$), this conclusion should remain valid in a broad range of debonding conditions. However, it is also clear from fig. 5 that there is a systematic tendency of the calculated force to overestimate the experimental values. In 36 experiments out of the 42, $F_{\max,\text{calc}}$ overestimates $F_{\max,\text{obs}}$ by a factor between 1.2 and 2.5. As mentioned above, this may be assigned to the machine compliance and the paste compressibility, which offset the position of the force maximum (ideally at $t = 0$ and $h = h_0$) along the force decay curve.

On this basis, the next step is to look for correlations between the maximum pressure drop values Δp_{\max} , calculated from $F_{\max,\text{obs}}$, and the failure mode. The results are summarized in fig. 6. As far as the average value for each mode, $\langle \Delta p_{\max} \rangle_i$, with $i = A, B$ or *C*, is concerned, the trend is now clear. In spite of a rather broad distribution of values for each mode, $\langle \Delta p_{\max} \rangle$ increases as one goes from mode *A* to mode *B* and to mode *C* (−2.1, −27.4 and −33 kPa, respectively). A similar evolution is observed for the smallest Δp_{\max} values at which a given failure mode starts to be observed. Mode *A* may be observed at vanishingly small pressure drops, as expected for simple flow of

a fluid without yield stress, whereas a pressure drop larger than -10^4 or $-2 \cdot 10^4$ Pa has to be reached for mode *B* or mode *C* to appear, respectively. The relatively small values of even the largest Δp_{\max} in the void-controlled failure modes (much less than atmospheric pressure) are in agreement with a heterogeneous cavitation mechanism, *i.e.* the growth of pre-existing bubbles. Homogeneous nucleation would imply much larger depressions.

The reason for the existence of a threshold Δp_{\max} value is not obvious. The pressure in any pre-existing bubble is larger than the atmospheric pressure and the pressure jump across the interface is given by the Laplace relationship, $\Delta p_{\text{Lap}} = 2\gamma/r$, in which γ is the liquid/vapor interface tension and r the mean curvature radius. Thus, any pressure drop induced by the traction force should allow the bubble to grow while decreasing its curvature and ultimately leading to failure. Our results show that this is not the case.

A clue comes from the threshold value of Δp_{\max} for mode *B* ($\sim -10^4$ Pa, fig. 6). Assuming that the interface tension is that of the wet air/water interface (0.076 N m^{-1}) that is, neglecting the possible surfactant effect of the polymers used in the preparation, the onset of failure mode *B* corresponds to the Laplace (or capillary) pressure across an interface with a mean curvature radius of $15 \mu\text{m}$. This is of the same order as the average grain radius in the paste. An exact correspondence should not be looked for, be it only for the interface tension assumption just made, but the order of magnitude information is significant. It suggests strongly that, indeed, the transition from type *A* to type *B* failure mode is controlled by the growth of bubbles the curvature of which is related to the dense granular structure of the medium. More precisely, it shows that the bubbles nucleate in the dispersing fluid of the paste, in the interstitial space between grains.

3.2 Tackiness

The total energy dissipated during the debonding experiment (the tackiness) is directly related to the shape of the force-strain curve. With PSA adhesives [11,15–17] and also with highly viscous Newtonian liquids in the cavitation regime [18,19], a rather complex force decay curve is observed beyond F_{\max} . Several features are observed, the most noticeable being a wide force plateau due to the smooth growth of the bubbles. This force plateau is the main contribution to tackiness. No such plateau has been observed in our experiments. The decay is always featureless and rapid.

In the following, we will analyze in more details the shape of the force decay curves obtained with the granular adhesive (sample P_β), where failure is always of type *C* in our experimental conditions. With a shear-thinning paste like this one, one expects the peak force to have only a weak dependence on the separation velocity (eq. (2)). This is confirmed by the velocity dependence of F_{\max} for the 14+7 experiments with the highest recording quality (test machine and rheometer) (fig. 7). The best fit of the data

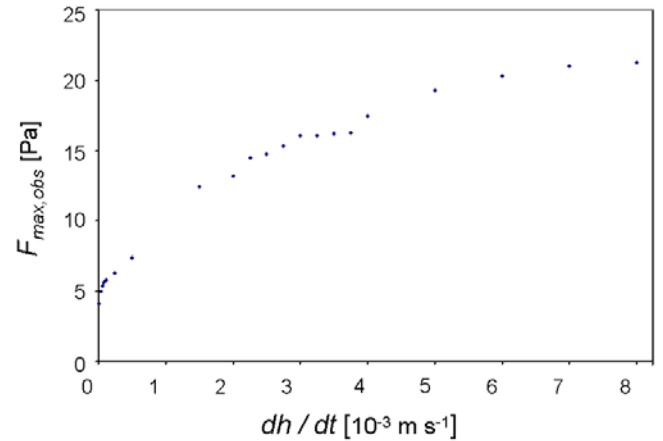


Fig. 7. Plate separation velocity dependence of the maximum pulling force. Two sets of data are shown on this graph: 1) data obtained with the test machine at relatively high separation velocity (from 1.5 to $8 \cdot 10^{-3} \text{ m s}^{-1}$) and 2) data obtained with the rheometer at much smaller velocity (below $0.6 \cdot 10^{-3} \text{ m s}^{-1}$).

leads to $F_{\max} \propto (dh/dt)^{0.34}$, very close to the shear rate dependence of the stress plateau values in fig. 2.

As far as the monotonous decay of the pulling force beyond the force peak is concerned, a good fit of these 7+14 data curves, recorded at small separation velocities, may be obtained by using an exponential decay:

$$F = F_{\max} \exp(-t/\tau_{\text{dec}}). \quad (4)$$

Significant departure from simple exponential behavior was observed with the 14 data curves obtained at higher velocity, using the test machine. A good fit could nevertheless be obtained using a stretched exponential decay:

$$F = F_{\max} \exp[-(t/\tau_{\text{dec}})^v], \quad (5)$$

with $v \geq 2$.

One possible physical origin for this characteristic time would be the intrinsic visco-elastic relaxation time(s) of the paste. However, as pointed out in the previous sections, this type of paste is characterized by its visco-plastic character rather than by its visco-elasticity. Thus, another possibility is that it merely reflects the time scale τ_{fl} of the viscoplastic flow as the plates are separated. This time scale may be defined as the inverse strain rate $\tau_{\text{fl}} = h_0/u = 1/\dot{\epsilon}_{zz}$ for instance. As shown in fig. 8, the correlation between τ_{dec} and τ_{fl} is indeed very good. The data used in fig. 8 are those obtained at relatively low velocity with the home-made setup. Thanks to the combined variation of initial thickness h_0 and separation velocity \dot{h} , a broad range of τ_{dec} values was obtained in this set of experiments, covering almost three orders of magnitude, from $\sim 5 \text{ s}$ to $\sim 4 \cdot 10^3 \text{ s}$. The correlation yields $\tau_{\text{dec}} \propto \tau_{\text{fl}}^{1.05}$. This means that the time- or displacement-dependence of the failure process is not related to a characteristic time of the fluid itself. It merely reflects the imposed strain rate.

This suggests that a master curve could be obtained by plotting F/F_{\max} as a function of t/τ_{dec} . Indeed, as illustrated in fig. 9, a reasonably good data collapse is obtained

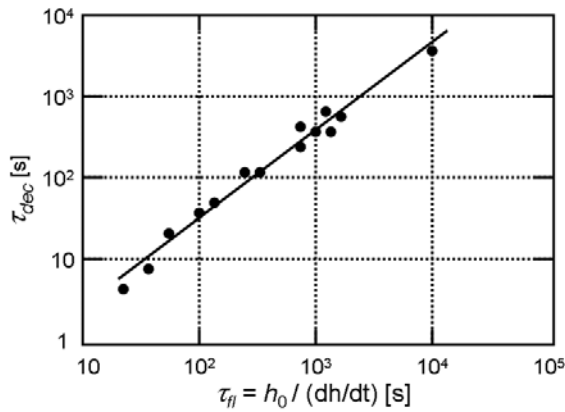


Fig. 8. Correlation between the characteristic time τ_{dec} of the exponential decay of the pulling force and the characteristic time $\tau_{fl} = h_0/u$ of the imposed separation velocity. The data shown are those obtained at relatively small velocities using paste P_β and the home-made setup.

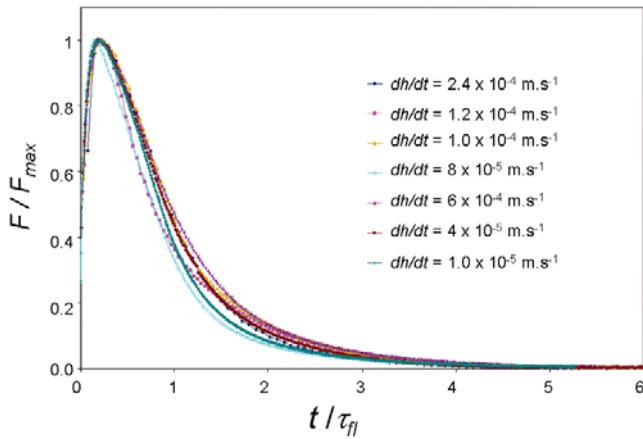


Fig. 9. Master curve obtained by collapsing the data curves recorded at small separation velocity using the AR2000 rheometer.

by using the data recorded at low velocity (the collapse is better with the data obtained at larger velocity with the test machine but, as pointed out above, the decay is stretched-exponential, which makes the physical interpretation more difficult).

3.3 Failure mechanism

Considering the good correlation between τ_{dec} and τ_{fl} , and the exponential or quasi-exponential character of the post-peak force decay, a first model would be to consider the failure process as a random process, with a constant probability $\dot{\epsilon}_{zz}$ for failure per unit time (or, equivalently, per incremental strain). More precisely, the bubble nucleation and growth could be modeled as a damage mechanism based on the capillary pressure as a damage criterion. The damage growth law then appears to be well described by a constant relative rate. Namely each element of volume has a constant probability per strain increment to experience a bubble expansion. Let D be the damage or equivalently,

the fraction of elements of volume which have “failed” due to the formation of a bubble. Once a bubble has been formed in a volume element, it releases the stress in its vicinity and kills the contribution of other nucleation sites above and below it. No further damage can occur within the same element. The damage rate, \dot{D} , or fraction of such “failed” element of volume is thus proportional to the total strain rate, and to the fraction of undamaged elements of volume, $(1 - D)$. It thus obeys $\dot{D} \propto (1 - D)\dot{\epsilon}$, hence $D = 1 - \exp(-\epsilon/\epsilon_0)$, where ϵ_0 is a characteristic strain. The corresponding macroscopic stress is then proportional to $(1 - D)$, and hence drops exponentially with the gap in between the plates. Let us note that the local stress in un-failed elements of volume is the macroscopic stress divided by $(1 - D)$, and thus remains constant within the entire plate separation, a hypothesis consistent with the fact that the local bubble generation criterion is based on a capillary pressure argument, which does not depend on the macroscopic damage state.

In spite of its simplistic character and the neglect of the increasingly elongational character of the flow in some regions, this model is in agreement with the main experimental observations (exponential decay; correlation between τ_{dec} and τ_{fl} ; plasticity). However, it does not describe neither the growth of bubbles up to macroscopic sizes, nor the formation of the large “valleys” which are visible in fig. 1. Nor does it explain the self-affine morphology of the interface that was previously evidenced [23].

Even more questionable is the assumption of a constant nucleation rate. Nucleation is triggered by the pressure drop, which depends on the strain and the strain rate. It decreases as the plate separation increases. Hence, among all the microbubbles initially trapped in the paste, only the most fragile, *i.e.* those with the smallest curvature will grow. They grow until they reach contact with the grains. Growth may then be stopped for a while as the interface adapts itself to the curvature of the grains. At this point the volume element in which the bubble is growing is considered as “damaged”. What is going on beyond that point is unclear. The bubbles may either grow as ordinary bubbles in a homogeneous fluid or, due to the high density of grains close to jamming, their growth may be hindered at least for some time. The interface could still advance by an invasion percolation mechanism in the interstitial space between the grains, just like in an unsaturated porous medium. Unfortunately, the opaque character of the pastes that we used is preventing any direct observation of what is really happening. Working with index-matched pastes would be extremely useful in that respect.

4 Conclusion

In this paper we have studied the cohesive failure of pasty granular materials in a simple pulling test performed on a layer of paste confined between rigid plates. It was shown that failure can take several forms, stemming from different mechanisms and leading to different failure surface

morphologies. Two main mechanisms have been identified: the first mechanism, similar to what is observed with simple viscous liquids at low debonding velocity, is inward flow in parallel to elongation. The second mechanism involves the growth of defects which were identified as interstitial microbubbles. The transition between the two regimes is controlled by the flow-induced pressure drop in the paste. This mechanism is akin to the mechanism leading to adhesive failure with soft polymer adhesives or with simple viscous liquids at high debonding velocity. The decay of the pulling force during the test supports a simple model of heterogeneous bubble nucleation and growth under a constant local depression.

References

1. E. Ben-Jacob, R. Godbey, N.D. Goldenfeld, J. Koplik, H. Levine, T. Muller, L.M. Sander, *Phys. Rev. Lett.* **55**, 1315 (1985).
2. H. La Roche, J.F. Fernandez, M. Octavio, A.G. Loeser, C.J. Lobb, *Phys. Rev. A* **44**, R6185 (1991).
3. J. Bohr, S. Brunak, T. Norretranders, *Europhys. Lett.* **25**, 245 (1994).
4. S. Tarafdar, S. Roy, *Fractals* **3**, 99 (1995).
5. S. Roy, S. Tarafdar, *Phys. Rev. E* **54**, 6495 (1996).
6. S. Kabira, S. Tarafdar, *Physica A* **328**, 305 (2003).
7. A. Lindner, D. Derks, J.M. Shelly, *Phys. Fluids* **17**, 072107 (2005).
8. M. Ben Amar, D. Bonn, *Physica D* **209**, 1 (2005).
9. P.G. Saffman, G.I. Taylor, *Proc. R. Soc. London, Ser. A* **245**, 312 (1958).
10. Q. Barral, G. Ovarlez, X. Chateau, J. Boujlel, B. Rabideau, P. Coussot, *Soft Matter* **6**, 1343 (2010).
11. C. Creton, *MRS Bull.* **28**, 434 (2003).
12. A. Zosel, *Adv. Pressure Sensitive Adhes. Technol.* **1**, 92 (1992).
13. A. Zosel, *J. Adhes.* **30**, 135 (1989).
14. H. Lakrout, P. Sergot, C. Creton, *J. Adhes.* **69**, 307 (1999).
15. C. Gay, L. Leibler, *Phys. Rev. Lett.* **82**, 936 (1999).
16. D. Derks, A. Lindner, C. Creton, D. Bonn, *J. Appl. Phys.* **93**, 1557 (2003).
17. C. Creton, H. Lakrout, *J. Polym. Sci. B* **38**, 965 (2000).
18. S. Poivet, F. Nallet, C. Gay, P. Fabre, *Europhys. Lett.* **62**, 244 (2003).
19. S. Poivet, F. Nallet, C. Gay, J. Teisseire, P. Fabre, *Eur. Phys. J. E* **15**, 97 (2004).
20. H. Van Damme, S. Mansoutre, P. Colombet, C. Lesaffre, D. Picart, *C. R. Physique* **3**, 229 (2002).
21. A. Kaci, R. Bouras, M. Chaouche, P.-A. Andréani, H. Brossas, *Appl. Rheol.* **19**, 51970 (2009).
22. A. Kaci, R. Bouras, V.T. Phan, P.-A. Andréani, M. Chaouche, H. Brossas, *Cem. Concr. Comp.* **33**, 218 (2011).
23. E. Lemaire, Y. Abdelhaye, J. Larue, R. Benoit, P. Levitz, H. Van Damme, *Fractals* **1**, 968 (1993).
24. H. Van Damme, E. Lemaire, Y.O.M. Abdelhaye, A. Mourchid, P. Levitz, in *Non-Linearity and Breakdown in Soft Condensed Matter*, edited by K.K. Bardan, B.K. Chakrabarti, A. Hansen, *Springer Lect. Notes Phys.*, Vol. **437** (Springer-Verlag, 1994) p. 134.
25. Y.O.M. Abdelhaye, M. Chaouche, H. Van Damme, *Appl. Clay Sci.* **42**, 163 (2008).
26. B.A. Francis, R.G. Horn, *J. Appl. Phys.* **89**, 4167 (2001).
27. J. Teisseire, F. Nallet, P. Fabre, C. Gay, *J. Adhes.* **83**, 613 (2008).
28. G.H. Meeten, *Rheol. Acta* **41**, 557 (2002).